Origin of kinks in the energy dispersion of strongly correlated matter

Kazue Matsuyama,[1] Edward Perepelitsky,[2,3] and B. Sriram Shastry[1]
[1]*Physics Department, University of California, Santa Cruz, California 95064, USA*
[2]*Centre de Physique Théorique, École Polytechnique, CNRS, Université Paris-Saclay, 91128 Palaiseau, France*
[3]*Collège de France, 11 place Marcelin Berthelot, 75005 Paris, France*
(Received 22 January 2017; published 20 April 2017)

We investigate the origin of ubiquitous low-energy kinks found in angle-resolved photoemission experiments in a variety of correlated matter. Such kinks are unexpected from weakly interacting electrons and hence identifying their origin should lead to fundamental insights in strongly correlated matter. We devise a protocol for extracting the kink momentum and energy from the experimental data which relies solely on the two asymptotic tangents of each dispersion curve, away from the feature itself. It is thereby insensitive to the different shapes of the kinks as seen in experiments. The body of available data are then analyzed using this method. We proceed to discuss two alternate theoretical explanations of the origin of the kinks. Some theoretical proposals invoke local bosonic excitations (Einstein phonons or other modes with spin or charge character), located exactly at the energy of observed kinks, leading to a *momentum-independent* self-energy of the electrons. A recent alternate is the theory of extremely correlated Fermi liquids (ECFL). This theory predicts kinks in the dispersion arising from a *momentum-dependent* self-energy of correlated electrons. We present the essential results from both classes of theories, and identify experimental features that can help distinguish between the two mechanisms. The ECFL theory is found to be consistent with currently available data on kinks in the nodal direction of cuprate superconductors, but conclusive tests require higher-resolution energy distribution curve data.

DOI: 10.1103/PhysRevB.95.165435

I. INTRODUCTION

High-precision measurements of electronic spectral dispersions have been possible in recent years, thanks to the impressive enhancement of the experimental resolution in the angle-resolved photoemission spectroscopy (ARPES). This technique measures the single-electron spectral function $A(\vec{k},\omega)$ multiplied by the Fermi occupation function; it can be scanned at either fixed $\vec{k}$ as a function of ω or at fixed ω as a function of $\vec{k}$. These scans produce, respectively, the energy distribution curves (EDCs) and momentum distribution curves (MDCs). The line shapes in both these scans are of fundamental interest since they provide a direct picture of the quasiparticle and background components of interacting Fermi systems, and thus unravel the roles of various interactions that are at play in strongly correlated Fermi systems. The dispersion relation of the electrons can be studied through the location of the peaks of $A(\vec{k},\omega)$ in constant ω or constant $\vec{k}$ scans.

Recent experimental studies have displayed a surprising ubiquity of *kinks* in the dispersion of strongly correlated matter at low energies ∼50–100 meV. The kinks are bending-type anomalies (see Fig. 1) of the simple $\omega = v_F(\vec{k} - \vec{k}_F)$, i.e., linear energy versus momentum dispersion that is expected near $\vec{k}_F$ from band theory. The special significance of kinks lies in the fact that their existence *must* signal a *departure* from band theory. This departure could be either due to electron-electron interactions or to interaction of the electrons with other bosonic degrees of freedom. Either of them are therefore significant enough to leave a direct and observable fingerprint in the spectrum. The goal of this work is to elucidate the origin of the observed kinks, and therefore to throw light on the dominant interactions that might presumably lead to high-T_c superconductivity.

The purpose of this paper is multifold: We (i) survey the occurrence of the kinks in a variety of correlated systems of current interest, (ii) provide a robust protocol for characterizing the kinks which is insensitive to the detailed shape of the kink, (iii) discuss how these kinks arise in two classes of theories, one based on coupling to a bosonic mode and the other to strong correlations, and (iv) identify testable predictions that ARPES experiments can use to distinguish between these.

The 15 systems reporting kinks are listed in Table I: these include (1) most high-T_c cuprates in the (nodal) direction $\langle 11 \rangle$ at various levels of doping from insulating to normal metallic states in the phase diagram [1,2], (2) charge density wave systems, (3) cobaltates, and (4) ferromagnetic iron surfaces. The kinks lose their sharpness as temperature is raised [2–4], and appear to evolve smoothly between the d-wave superconducting state and the normal state.

The kinks above T_c are smoothed out as one moves away from nodal direction [5]. Recent experiments [6] resolve this movement of the kinks more finely into two subfeatures. Most of the studies in Table I focus on MDC kinks; the EDC kinks data are available for only eight systems so far. Bosonic modes have been reported in six systems using different probes such as inelastic x rays or magnetic scattering, with either charge (phonons, plasmons) or spin (magnetic) character, while the remaining nine systems do not report such modes. A few theoretical studies of the kinks have implicated the observed low-energy modes via electron-boson–type calculations; we summarize this calculation in the Supplemental Material (SM) [7]. We find, in agreement with earlier studies, that the boson coupling mechanism yields kinks in the MDC dispersion, provided the electron-boson coupling is taken to be sufficiently large. In addition, we find in all cases studied this mechanism also predicts a jump in the EDC dispersion. It also predicts an extra peak in the spectral function pinned to the kink energy after the wave vector crosses the kink. These two features are experimentally testable and differ from the predictions of the correlations mechanism discussed next.

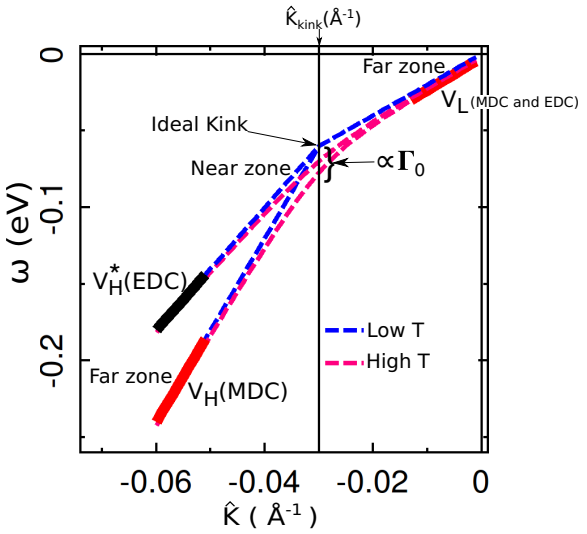

FIG. 1. A schematic MDC and EDC spectrum displaying typical features of experiments discussed below. Here, $\hat{k} = (\vec{k} - \vec{k}_F) \cdot \vec{\nabla}\varepsilon_{k_F}/|\vec{\nabla}\varepsilon_{k_F}|$ is the momentum component normal to the Fermi surface, and we label EDC variables with a star. [The sketch uses parameters $V_L = 2$ eV Å, $V_H = 6$ eVÅ, $r = 1.5$, $\hat{k}_{\rm kink} = -0.03$ Å^{-1}, $\Delta_0 = 0.03$eV, and $\Gamma_0 = 0.01$eV in Eqs. (3) and (4).] The tangents in the *far zones* identify the asymptotic velocities $V_L < V_H$ and $V_L^* < V_H^*$ that characterize the MDC and EDC spectra. The intersection of the extrapolated MDC tangents fixes the kink momentum $\hat{k}_{\rm kink}$ and the ideal energy $E^{\rm ideal}_{\rm kink}$. The dispersion is rounded with raising T, as in the lower (red) curve. We *define* the MDC kink energy $E^{\rm MDC}_{\rm kink}$ as $E(\hat{k}_{\rm kink})$, i.e., the binding energy measured *at* the kink momentum, and similarly the EDC kink energy. In all cases, $V_L = V_L^*$. A testable consequence of the ECFL theory is that V_H^* is fixed in terms of the two MDC velocities by a strikingly simple relation: $V_H^* = \frac{3V_H - V_L}{V_H + V_L} \times V_L$ [see Eq. (10)]. This easily testable prediction is tried against experimental data in Fig. 2 where both EDC and MDC data are available. In contrast, the electron-boson theory predicts a jump in the EDC dispersion at the kink energy, followed by $V_H^* = V_H$. Note that the difference between the EDC (MDC) kink energy, $E^{EDC}_{\rm kink} = E^{\rm ideal}_{\rm kink} - \Gamma_0$ and $E^{\rm MDC}_{\rm kink} = E^{\rm ideal}_{\rm kink} - \Gamma_0\sqrt{\frac{r}{2-r}}$, and the ideal kink energy is equal (proportional) to Γ_0.

Since kinks are also observed in cases where no obvious bosonic mode is visible, it is important to explore alternate mechanisms that give rise to such features. In this context, we note that a recent theoretical work using the extremely strongly correlated Fermi liquid (ECFL) theory [8,9] calculates the dispersion using low-momentum and frequency expansions of the constituent self-energies. This calculation [9] shows that both EDC and MDC energy dispersions display qualitatively similar kinks, in particular, there is no jump in either dispersion. In essence, this work implies that a purely electronic mechanism with a strong momentum dependence of the Dyson self-energy results in kink-type anomalies. In terms of parameter counting, the calculation is *overdetermined*; it can be represented in terms of four parameters which can be fixed from a subset of measurements. With this determination one can then predict many other measurables and testable relations between these, as we show below. We show below that the various predictions are reasonably satisfied in one case (of OPT Bi2212 below), while in other cases, there are insufficient experimental data to test the theories.

The ECFL theory incorporates strong Gutzwiller-type correlation effects into the electron dynamics [7]. It produces line shapes that are in close correspondence to experimental results for the high-T_c systems [11,12]. The presence of a low-energy kink in the theoretical dispersion was already noted in Ref. [11]; this work substantially elaborates that observation. In order to understand the origin of a low-energy scale in the ECFL theory, it is useful to recall the predicted cubic correction to Fermi liquid self-energy $\mathrm{Im}\,\Sigma(\vec{k}_F,\omega) \sim \omega^2(1 - \frac{\omega}{\Delta_0})$ from equations (SM-42) and (8) and (9). Here, Δ_0 is an emergent low-energy scale; it is related to the correlation-induced reduction of the quasiparticle weight Z. It reveals itself most clearly in the observed particle-hole asymmetry of the spectral functions, and therefore can be estimated independently from spectral *line-shape* analysis. A related and similar low value of the effective Fermi temperature is found in recent studies of the resistivity [10]. Here and in our earlier studies it is coincidentally found that $\Delta_0 \sim 20$–50 meV, i.e., it is also roughly the energy scale of the kinks when the bandwidth is a few eV.

II. ARPES SPECTRAL DISPERSIONS, KINKS, AND A PROTOCOL FOR DATA ANALYSIS

A. Summary of variables in the theory

A few common features of spectral dispersions found in experiments are summarized in Fig. 1. The schematic figure shows a region of low spectral velocity near the Fermi level followed by a region of steeper velocity; these are separated by a bend in the dispersion, namely, the kink. While the kink itself has a somewhat variable shape in different experiments, the "far zone" is much better defined and is usually independent of the temperature; we denote the velocities in the far zones V_L, V_H for the MDC dispersion and the EDC dispersion counterparts by V_L^*, V_H^*. In terms of the normal component of the momentum measured from the Fermi surface

$$\hat{k} = (\vec{k} - \vec{k}_F).\vec{\nabla}\varepsilon_{k_F}/|\vec{\nabla}\varepsilon_{k_F}|, \tag{1}$$

the kink momentum $\hat{k}_{\rm kink}$ is uniquely defined by extrapolating the two asymptotic tangents, and the binding energy at this momentum defines the ideal kink energy $E^{\rm ideal}_{\rm kink}$ [see Eq. (7)], which serves as a useful reference energy.

Our picture is that all lines of temperature-varying MDC dispersion curves in near zone converges into one line in the far zone in Fig. 1. We find that both the low and high velocities are independent of the temperature while depending on the doping levels. Lastly, the new laser ARPES data reveal that we need low-temperature dispersion data to determine V_L because temperature effect strongly influences the spectrum near the Fermi level.

We first define the important ratio parameter r ($1 \leqslant r \leqslant 2$) from the MDC dispersion velocities as

$$r = \frac{2V_H}{V_H + V_L}. \tag{2}$$

The EDC dispersion relation $E^*(\hat{k})$ locates the maximum of the spectral function $A(\vec{k},\omega)$ in ω at constant $\hat{k}$, while the MDC

TABLE I. Comprehensive survey for ARPES kinks.

	Above T_c		Below T_c		Local bosonic mode		
Name of the compounds	MDC	EDC	MDC	EDC	Charge	Spin	Not reported
LSCO	✓[3,13]		✓[1,3,13,14]	✓[15]	✓[16–18]	✓[19]	
Bi2201	✓[3,5,13,20,21]	✓[23]	✓[5,21]		✓[24]		
Bi2212	✓[2–5,13,25,26]	✓[4]	✓[2–5,13,25,26]		✓[27]	✓ [28,29]	
Bi2223	✓[5,30]		✓[5,30,31]				✓
YBCO			✓[32]		✓[33,34]	✓[35–38]	
Hg1201			✓[39]		✓[40]	✓[41–43]	
F0234			✓[44]				✓
CCOC			✓[45]				✓
LSMO			✓[46]	✓[46]			✓
2H-TaSe2 (CDW)			✓[47]		✓[48]		
Iron (110) surface			✓[49]				✓
BiBaCo1			✓[50] 5 K	✓[50] 5 K			✓
BiBaCo2			✓[50] 5 K	✓[50] 5 K			✓
BiBaCo	✓[50] 200 K	✓[50] 200 K					✓
NaCoO			✓[50] 5 K	✓[50] 5 K			✓

dispersion and $E(\hat{k})$ locates the maximum $\hat{k}$ at a fixed energy ω. These are found from the ECFL theory (see SM [7] and Ref. [9]) as

$$E^*(\hat{k}) = \left(r\, V_L \hat{k} + \Delta_0 - \sqrt{\Gamma_0^2 + Q^2}\right), \tag{3}$$

$$E(\hat{k}) = \frac{1}{2-r}\left(V_L \hat{k} + \Delta_0 - \sqrt{r(2-r)\,\Gamma_0^2 + Q^2}\right), \tag{4}$$

where we introduced an energy parameter related to r, V_L and $\hat{k}_{\rm kink}$

$$\Delta_0 = \hat{k}_{\rm kink} V_L (1-r), \tag{5}$$

and a momentum-type variable $Q = (r-1)\, V_L\, (\hat{k} - \hat{k}_{\rm kink})$. The variable Γ_0 is temperaturelike

$$\Gamma_0 = \eta + \pi \{\pi k_B T\}^2 / \Omega_\Phi; \tag{6}$$

η is an elastic scattering parameter dependent upon the incident photon energy, and η is very small for laser ARPES experiments and can be neglected to a first approximation. Here, Ω_Φ is a self-energy decay constant explained further in the SM [7]. The ideal kink energy $V_L \hat{k}_{\rm kink}$ can be expressed in terms of Δ_0 scale as

$$E_{\rm kink}^{\rm ideal} = -\frac{1}{r-1}\Delta_0. \tag{7}$$

It is important to note that these dispersion relation equations (3) and (4) are different from the standard dispersion relations $E_{\rm FLT}(\hat{k}) = E^*_{\rm FLT}(\hat{k}) = V_H \hat{k}$, which follow in the simplest Fermi liquid theory (FLT) near the Fermi energy $A_{\rm FLT}(\vec{k},\omega) = \frac{1}{\pi}\frac{\Gamma_0}{(\omega - V_H \hat{k})^2 + \Gamma_0^2}$. The FLT dispersions are identical in EDCs and MDCs, and are independent of the temperaturelike variable Γ_0, and do not show kinks. On the other hand, Eqs. (3) and (4) do have kinks, as we show below, and the temperaturelike variable Γ_0 plays a significant role in the dispersion. At $\Gamma_0 = 0$ one has an ideal spectrum, where the kinks are sharpest. When $\Gamma_0 \neq 0$, due to either finite temperature or finite damping η, related to the energy of the incoming photon, the kinks are rounded.

A few consequences of Eqs. (3) and (4) can be noted for the purpose of an experimental determination of the Fermi momentum. The chemical potential is usually fixed by referencing an external metallic contact and is unambiguous. Experimentally, the Fermi momentum is usually found from the MDC, as the momentum where the spectral function is maximum with energy fixed at the chemical potential, i.e., $\omega = 0$. This corresponds to the generally wrong expectation that $E(\hat{k}_{\rm peak}) = 0$ implies $\hat{k}_{\rm peak} = 0$. When $\Gamma_0 \geqslant 0$, from Eq. (4) we see that the condition $E(\hat{k}_{\rm peak}) = 0$ gives $\hat{k}_{\rm peak} = \frac{\sqrt{\Delta_0^2 + r^2\,\Gamma_0^2} - \Delta_0}{r V_L}$, a positive number that equals zero only in the ideal case $\Gamma_0 = 0$. Thus, there is an apparent enlargement of the Fermi surface due to a finite Γ_0 that needs to be corrected. By the same token, at the true (Luttinger theorem related) Fermi momentum $\hat{k} = 0$, the MDC energy $E(0) = \frac{\Delta_0 - \sqrt{\Delta_0^2 + r(2-r)\Gamma_0^2}}{2-r}$, a negative number when $\Gamma_0 \neq 0$. In recent laser ARPES Bi2201 data [[21], panel (a) in Fig. 4], we see that $E(\hat{k}_{\rm peak})$ vanishes at increasing $\hat{k}_{\rm peak}$ as T is raised, as predicted in our calculation. Recent laser ARPES experiment on OPT Bi2212 compounds reports a similar temperature dependence of momentum of MDC dispersion at the Fermi level in Ref. [26], strongly supporting our picture of its origin.

Similarly, the EDC peak at the true Luttinger theorem related Fermi surface $\hat{k} = 0$ is nonzero. We find $E^*(0) = (\Delta_0 - \sqrt{\Delta_0^2 + \Gamma_0^2}) \leqslant 0$. Clearly, $E^*(0)$ is negative unless $\Gamma_0 = 0$, i.e., it is generically red-shifted. If we are tempted to identify the Fermi momentum from the condition $E^*(\hat{k}^*_{\rm peak}) = 0$, a similar cautionary remark is needed. The condition $E^*(\hat{k}^*_{\rm peak}) = 0$ gives $\hat{k}^*_{\rm peak} = \frac{\sqrt{\Delta_0^2 + (2r-1)\Gamma_0^2} - \Delta_0}{(2r-1)V_L}$, again a positive number as in the MDC case, and thus a slightly different enlargement of the apparent Fermi surface.

The above comments illustrate the difficulty of finding the correct Fermi surface when Γ_0 is non-negligible, as in the case of synchrotron ARPES with substantial values $\Gamma_0 \gtrsim 50$ meV. On the other hand, the laser ARPES studies have a much smaller $\eta \lesssim 10$ meV, where our analysis can be tested by varying the temperature and the consequent change of the

spectrum. In the following, we analyze the data from the Bi2201 system where the laser data are available at various T, and allows us to test the above in detail. Our analysis below of two other synchrotron data, the OPT Bi2212 has $10 \leqslant \eta \leqslant 40$ meV, while the low-T LSCO data are assumed to be in the limit of $\eta = 0$ because of the lack of high-temperature dispersion data.

The spectral function at low frequencies close to $\vec{k}_F$ is also obtainable from these parameters; the relevant formula is noted below. In terms of ξ

$$\xi = \frac{1}{\Delta_0}(\omega - r\, V_L \hat{k}) \tag{8}$$

the spectral function is

$$A(\vec{k},\omega) = \frac{z_0}{\pi} \frac{\Gamma_0}{(\omega - V_L\hat{k})^2 + \Gamma_0^2} \left\{ 1 - \frac{\xi}{\sqrt{1 + c_a \xi^2}} \right\}. \tag{9}$$

Here, z_0 is the quasiparticle weight and $c_a \sim 5.4$ (see SM [7]). We should keep in mind that these expressions follow from a low-energy expansion, and is limited to small $\hat{k}$ and ω; in practical terms the dimensionless variable $|\xi| \lesssim 4$, so that ω (or $\hat{k}$) is bounded by the kink energy (or momentum), as defined below. Finally, we note a strikingly simple relation that relates the high velocity of the EDC spectrum to the two velocities V_H and V_L in the MDC dispersion defined in Fig. 1:

$$V_H^* = \frac{3V_H - V_L}{V_H + V_L} \times V_L. \tag{10}$$

The origin of this simple but *key formula* lies in the fact that the entire ECFL spectrum is determined in terms of a few parameters, and therefore one should expect inter-relationships of this kind on general grounds. The details are provided in the Supplemental Material [7] Eq. (SM-36).

III. OPT BI2212 ARPES DISPERSION DATA

In the well-studied case of optimally doped Bi2212 (BSCCO) superconductors, the kink has been observed in both EDC and MDC. We summarize the ECFL fit parameters in Table II obtained from literature [4]. We also display the predicted energy and high velocity of the EDC dispersion. The velocity ratio $V_H / V_H^* \sim 1.3$ in this case is quite large and measurable. In this case, the EDC dispersion has fortunately already been measured, allowing us to test the prediction. From Table II we see that the energy of the EDC kink and its velocity are close to the predictions.

In Fig. 2(a), we plot the predicted EDC dispersion using the parameters extracted from the MDC dispersion in Fig. 2(b), and compare with the ARPES data measured [4]. It is interesting that the predicted slope of the EDC dispersion from Eq. (10) is close to the measured one. Indeed, the measured EDC dispersion is close to that expected from the ECFL theory. To probe further, in Fig. 2(c) we compare the theoretical EDC line shape (solid blue line) given by the same parameters through Eq. (9) with the ARPES line shape measured at high temperature [4]. Figure 2(d) compares the theoretical MDC curve with the data. The theoretical curves are from the low-energy expansion and hence are chopped at the high end, corresponding to roughly $|\xi|_{\max} \sim \frac{r\, V_L \hat{k}_{\rm kink}}{\Delta_0}$ for MDC and $|\xi|_{\max} \sim \frac{E^{\rm ideal}_{\rm kink}}{\Delta_0}$ for the EDC. With this cutoff, the momentum is less than the kink momentum and the energy is less than the kink energy. We used $\Gamma_0 = 40$ meV since it provides a rough fit for both EDC and MDC spectral functions.

This value is somewhat larger than the bound $\sim$10 meV given in Table II; a smaller value leads to narrower lines but with the same shape. In rigorous terms, the same Γ_0 must fit the dispersion and also the spectral functions. Our fit, requiring a different Γ_0, is not ideal in that sense. However, the resolution of the available data is somewhat rough, and should improve with the newer experimental setups that have become available. We thus expect that higher-resolution data with laser ARPES should provide an interesting challenge to this theory. We also stress that from Eq. (9), the MDC line shapes look more symmetric than the EDC line shapes at low energies. While many experimental results do show rather symmetric MDCs, there are well-known exceptions. For instance, MDCs asymmetry has indeed been reported for nearly optimally doped Hg1201 ($T_c = 95$ K) at binding energy very close to the Fermi level, $\omega \sim -5$ meV and $\omega \sim -18$ meV in Fig. 5 in Ref. [39]. Note that the $\omega = 0$ MDC plot of the spectral function $A(k,\omega)$ from Eq. (9) locates the peak momentum $\hat{k}_{\rm peak} > 0$, i.e., slightly to the right of the physical Fermi momentum $\vec{k}_F$, and we consider this implies that the *experimental* Fermi momentum determination is subject to such a correction, whenever the spectral function Eq. (9) has a momentum-dependent caparison factor (see caption in Fig. 2).

TABLE II. Parameter table for ARPES kink analysis for OPT Bi2212 [4] in Fig. 2 presents three essential parameters: V_L, V_H, and $\hat{k}_{\rm kink}$. From the high- and low-temperature MDC dispersions, we measured $\Gamma_0 \lesssim 10$ meV in Fig. 2(b). With the measured experimental parameters and determining the velocity ratio r in Eq. (2), we are able to estimate the finite-temperature kink energy for EDC and MDC dispersions by $E^{\rm EDC}_{\rm kink} = E^{\rm ideal}_{\rm kink} - \Gamma_0$ and $E^{\rm MDC}_{\rm kink} = E^{\rm ideal}_{\rm kink} - \Gamma_0\sqrt{\frac{r}{2-r}}$ and predict V_H^* by $V_H^* = \frac{3V_H - V_L}{V_H + V_L} \times V_L$ in Eq. (10). The uncertainties for calculated variables were determined by error propagation, and the uncertainties for experimental variables were given by the half of the instrumental resolution.

MDCs					EDCs			
OPT Bi2212 ARPES data			$E^{\rm MDC}_{\rm kink}$ (meV)		$E^{\rm EDC}_{\rm kink}$ (meV)		V_H^* (eV Å)	
V_L (eV Å)	V_H (eV Å)	$\hat{k}_{\rm kink}$ (Å^{-1})	Calculated	Measured	Calculated	Measured	Predicted	Measured
1.47 ± 0.07	3.3 ± 0.3	-0.037 ± 0.005	67 ± 21	67 ± 8	63 ± 21	65 ± 8	2.60 ± 0.56	2.1 ± 1.1

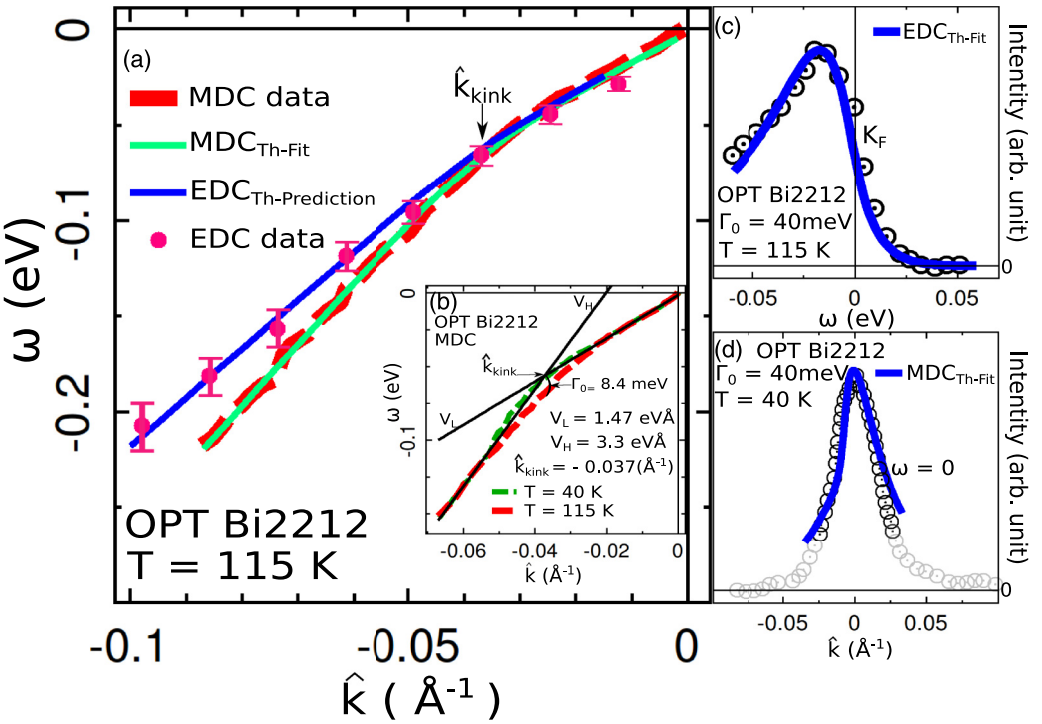

FIG. 2. ARPES kinks data for OPT Bi2212 from Ref. [4] compared to theoretical ECFL curves (solid lines) using parameters listed in Table II. (a) The predicted EDC spectrum (blue) from Eq. (3) versus the experimental EDC data (magenta symbols) at $T = 115$ K. For reference we also show the MDC data (red dashed curve) and the corresponding ECFL fit (green solid curve). (b) Experimental MDC spectra at 40 K (below T_c in green dashed line) and 115 K (above T_c in red dashed line) yield common asymptotes shown in black lines from the far zone. These determine the parameters displayed in Table II. (c) At low energy ±60 meV, the EDCs spectral function (blue solid line) from Eq. (9) is contrasted with the corresponding ARPES data from [4]. (d) At $\omega = 0$ we compare the MDCs spectral function (blue solid line) from Eq. (9) with the corresponding ARPES data from Ref. [4]. The range of validity for the theoretical expansion is $\pm\hat{k}_{\rm kink}(0.037\ \text{Å}^{-1})$, the data points in the range are shown in black circle symbols, while the light gray circle symbols are outside this range. The peak position of the theoretical curve has been shifted to left by 0.007 Å^{-1}, a bit less than the instrumental resolution. A similar shift is made in Fig. 3(l). For analogous reasons, the EDC peak in $A(k,\omega)$ at k_F is shifted to the left, i.e., $E^*(0) \leqslant 0$. A small shift to the *right* is made in Fig. 3(k), in order to compensate for this effect. These shift effects are within the resolution with present setups, but should be interesting to look for in future generation experiments since they give useful insights into the energy momentum dependence of the spectral function.

IV. LSCO LOW-TEMPERATURE DATA

Here, we analyze the LSCO data at low temperature (20 K) and at various doping levels raging from the insulator ($x = 0.03$) to normal metal ($x = 0.3$) from Ref. [1]. The parameters are listed in Table III, where we observe that the velocity V_L is roughly independent of x, and has a somewhat larger magnitude to that in OPT Bi2212 in Table II. The kink momentum decreases with decreasing x, roughly as $\hat{k}_{\rm kink} = -(0.37x - 0.77x^2)$ Å^{-1}, and the kink energies of EDC and MDC dispersions are essentially identical. In the region beyond the kink, the prediction for V_H^* is interesting since it differs measurably from the MDC velocity V_H. We find the ratio $V_H/V_H^* \sim 1.02$–1.5 is quite spread out at different doping.

Our analysis becomes unreliable as lower doping level $x < 0.075$ in Figs. 3(h)–3(j), where the dispersion kink is no longer a simple bending kink, an extra curving tendency begins to appear. To put this in context, recall that the line shape of LSCO becomes extremely broad at small x [14], and so the peak position of the spectral function becomes more uncertain than at higher energy.

We should point out that in Fig. 3(k) the spectral function has been shifted to right by 4 meV for a better fit. This shifting is consistent with our argument that the Fermi momentum determination has a possible small error of in order 0.006 Å^{-1}, arising from the $\hat{k}$-dependent caparison factor, and hence the peak position has an uncertainty $V_L \times 0.006 \sim 10$ meV.

V. BI2201 LASER ARPES DATA

In this section, we present our analysis of the high-resolution laser ARPES data of the single-layered compounds Bi2201, at various different doping levels taken from a recent study in Ref. [21]. In earlier studies of this compound using synchrotron emitted high-energy photons, as also LSCO [3], the ARPES kinks were observed to have only a weak temperature dependence [5]. However, the new high-resolution laser ARPES data enables us to observe clear and significant temperature dependence of the ARPES kinks; it is comparable to that of the double-layered Bi2212 compounds. In fact, we find that the new data of Bi2201 compounds in Ref. [21] seem to provide a textbook example of our ECFL kink analysis.

TABLE III. Data table for ARPES kink analysis for OPT LSCO ($T = 20$ K) [1] in Fig. 3. We were unable to reliably estimate Γ_0 here due to the lack of data at high temperature, and hence set it at zero. The uncertainties for measured values were given by half of the instrumental resolution (10 meV, $\sim$0.005 Å^{-1}). The uncertainties for the calculated values were determined by error propagation.

MDCs						EDCs			
LSCO low-temperature ARPES data				$E^{\rm MDC}_{\rm kink}$ (meV)		$E^{\rm EDC}_{\rm kink}$ (meV)		V^*_H (eV Å)	
x (doping level)	V_L (eV Å)	V_H (eV Å)	$\hat{k}_{\rm kink}$ (Å^{-1})	Calculated	Measured	Calculated	Measured	Calculated	Measured
0.3	2.4 ± 0.2	3.0 ± 0.3	-0.047 ± 0.005	113 ± 29	110 ± 10	113 ± 29		2.93 ± 0.45	
0.22	2.0 ± 0.1	3.6 ± 0.2	-0.042 ± 0.005	84 ± 18	85 ± 10	84 ± 18		3.14 ± 0.35	
0.18	1.7 ± 0.3	4.5 ± 0.6	-0.040 ± 0.005	68 ± 43	72 ± 10	68 ± 43		3.2 ± 1.2	
0.15	1.75 ± 0.07	4.3 ± 0.1	-0.037 ± 0.005	65 ± 11	64 ± 10	65 ± 11		3.23 ± 0.20	
0.12	2.0 ± 0.3	3.7 ± 0.5	-0.029 ± 0.005	58 ± 28	55 ± 10	58 ± 28		3.19 ± 0.89	
0.1	1.8 ± 0.2	5.0 ± 0.7	-0.035 ± 0.005	63 ± 44	64 ± 10	63 ± 44		3.5 ± 1.4	
0.075	1.9 ± 0.2	5.6 ± 0.8	-0.026 ± 0.005	49 ± 37	51 ± 10	49 ± 37		3.8 ± 1.7	
0.063	1.8 ± 0.3	6.0 ± 0.5	-0.022 ± 0.005	40 ± 21	43 ± 10	40 ± 21		3.7 ± 1.1	
0.05	1.7 ± 0.2	5.7 ± 0.6	-0.023 ± 0.005	39 ± 25	41 ± 10	39 ± 25		3.5 ± 1.3	
0.03	2.0 ± 0.3	6.1 ± 0.4	-0.016 ± 0.005	32 ± 15	32 ± 10	32 ± 15		4.02 ± 0.85	

In Table IV, we list the kink parameters corresponding to different doping levels of Bi2201 and tabulate the kink parameters. The entries are in correspondence to the panels in Fig. 4. In Figs. 4(a)–4(f), we depict the measured MDC dispersion and the predicted EDC dispersions at different doping levels. The latter are found from Eq. (3) using the variables in Table IV. Figures 4(g) and 4(h) of OPT Bi2201 are especially interesting. Combining the low $T = 15$ K dispersion data and the finite-T value of Γ_0, found from the depression of the kink energy $E^{\rm MDC}_{\rm kink} = E^{\rm ideal}_{\rm kink} - \Gamma_0\sqrt{\frac{r}{2-r}}$, we can reconstruct the entire MDC dispersion at a finite T. This may be compared with the measured finite-T MDC data, thus checking the validity of the formalism. This exercise is carried out at $T = 200$ K in Fig. 4(g) and $T = 100$ K in Fig. 4(h), where we find a remarkably good fit in all details. In Figs. 4(g) and 4(h) we show the actual momentum (rather than $\hat{k}$) to facilitate a comparison with data. Figure 4(g) especially clearly shows that $E(\hat{k})$ vanishes at a $\hat{k}$ that is different from 0. The shift corresponds to $\sim$0.01 Å^{-1}. We have commented above that this apparent expansion of the Fermi surface with T is due to the nontrivial physics underlying Eq. (4) lying beyond the simple minded FLT.

Figure 4(i) plots the temperature dependence of Γ_0 in Fig. 4(a) in Ref. [21]. The measured Γ_0 curve is fitted with Eq. (6), and we estimate $\eta = 5.3 \pm 2$ meV and $\Omega_\Phi = 410 \pm 100$ meV.

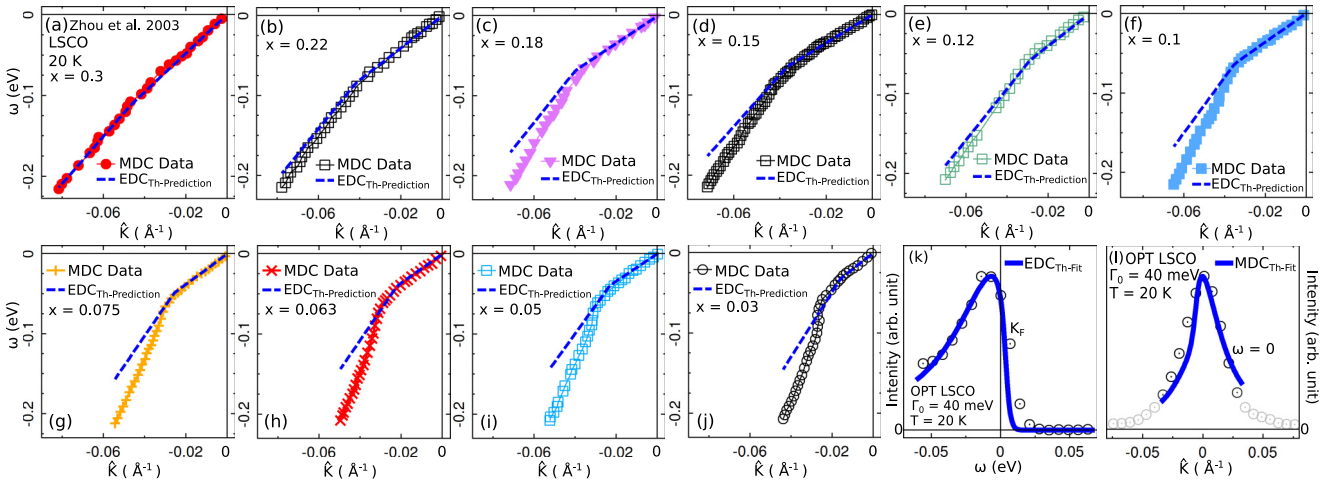

FIG. 3. ARPES kinks data for LSCO data [1] compared to theoretical ECFL curves (solid lines) using parameters listed in Table III. The doping level x varies between (normal metal) $0.3 \leqslant x \leqslant 0.03$ (insulator) in (a)–(j). Each panel shows MDC nodal dispersion data (symbols), whose uncertainties are $\pm$10 meV. The blue dashed line is the theoretical prediction for EDC dispersion by Eq. (3). (k) We compare the spectral line shape for EDCs at k_F from Eq. (9) (blue solid line) in the range $\pm E^{\rm ideal}_{\rm kink} \sim 65$ meV with the corresponding ARPES data (black circles) [12]. (l) At $\omega = 0$ we compare the MDCs spectral function (blue solid line) from Eq. (9) with the corresponding ARPES data from Ref. [12]. The range of validity for the theoretical expansion is $\pm\hat{k}_{\rm kink}$ (0.037 Å^{-1}), the data points in the range are shown in black circle symbols, while the light gray circle symbols are outside this range. The peak position of the theoretical curve MDC has been shifted to left by 0.006 Å^{-1}.

TABLE IV. Parameter table for ARPES kink analysis for laser ARPES data of Bi2201 at various different doping levels [21] in Fig. 4. From $0.1 < x < 0.16$, we measured $\Gamma_0 \sim 0$. For $x = 0.23$ and 0.26, we measured $\Gamma_0 \lesssim 17$ meV. For $x = 0.16$ data, we report variables for high-temperature kinks data 200 K (g) and 100 K (h) in Fig. 4, and Γ_0 values for 200 K and 100 K data are in corresponding panels (g) and (h) in Fig. 4. The uncertainties for the calculated parameters were determined by error propagation, and the uncertainties for the experimental parameters were given by half of the instrumental resolution.

MDCs						EDCs			
Bi2201 laser ARPES data				$E_{\rm kink}^{\rm MDC}$ (meV)		$E_{\rm kink}^{\rm EDC}$ (meV)		V_H^* (eV Å)	
x (doping level)	V_L (eV Å)	V_H (eV Å)	$k_{\rm kink}$ (Å^{-1})	Calculated	Measured	Calculated	Measured	Calculated	Measured
0.1	1.47 ± 0.12	4.7 ± 0.3	-0.022 ± 0.002	32 ± 3	37 ± 0.5	32 ± 6		3.0 ± 0.3	
0.11	1.34 ± 0.06	2.78 ± 0.06	-0.021 ± 0.002	28 ± 1	28 ± 0.5	28 ± 4		2.28 ± 0.12	
0.13	1.37 ± 0.07	2.71 ± 0.18	-0.025 ± 0.002	38 ± 3	39 ± 0.5	37 ± 5		2.27 ± 0.17	
0.16	1.5 ± 0.1	3.5 ± 0.2	-0.026 ± 0.002	39 ± 3	43 ± 0.5	39 ± 6		2.7 ± 0.2	
0.23	2.1 ± 0.11	5.4 ± 0.3	-0.036 ± 0.002	98 ± 6	97 ± 0.5	89 ± 10		3.9 ± 0.3	
0.26	2.17 ± 0.16	4.8 ± 0.4	-0.045 ± 0.002	123 ± 11	122 ± 0.5	114 ± 18		3.8 ± 0.4	
0.16 (200 K)	1.61 ± 0.18	3.5 ± 0.3	0.364 ± 0.002	87 ± 11	89 ± 0.5	75 ± 11		2.8 ± 0.4	
0.16 (100 K)	1.61 ± 0.18	3.5 ± 0.3	0.364 ± 0.002	69 ± 11	70 ± 0.5	62 ± 11		2.8 ± 0.4	

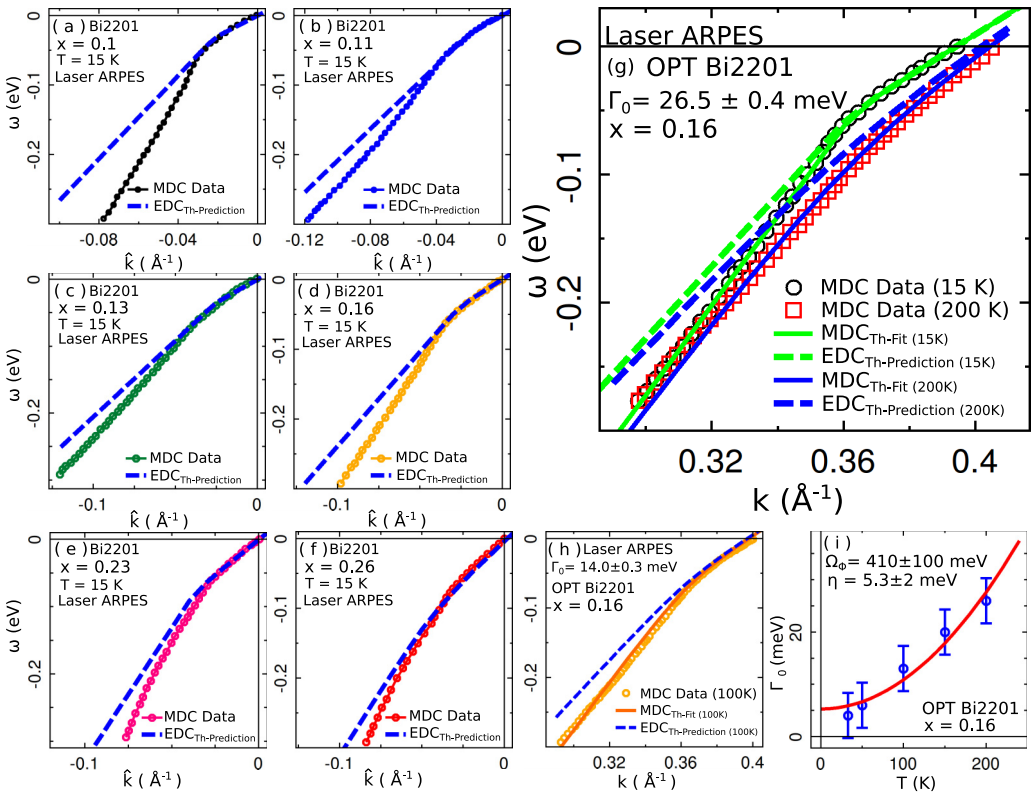

FIG. 4. ARPES kink analysis for laser ARPES data of Bi2201 at various different doping levels in Ref. [21]. (a)–(f) We predict EDC dispersions (blue dashed lines) using Eq. (3) for various different doping levels of Bi2201 laser ARPES data. (g), (h) First in (g), we present ECFL MDC fit (green solid line) for low-temperature (15 K) laser ARPES dispersion data of OTP Bi2201 from in Fig. 4(a) in Ref. [21] (black circles) and predict low-temperature EDC dispersion (green dashed line). Next, in (g) and (h), we predict high-temperature EDC (blue dashed lines) dispersions (g) 200 K and (h) 100 K for laser ARPES data of OPT Bi2201 [Fig. 4(a) in Ref. [21]], and show the MDC dispersion fits for two temperatures also, blue solid line for 200-K data (red squares) in (g) and brown sold line for 100-K data (yellow circles) in (h). We estimate Γ_0 from measuring the difference between the ideal kink energy and the MDC kink energy. In order to compare with experiments, the x-axis representation in (g) and (h) is given by the physical k (rather than the momentum difference $\hat{k}$). In (g), the MDC dispersion fit (blue solid line) of 200 K vanishes at $k = 0.404 \pm 0.002$ Å^{-1}, very close to the measured $k = 0.405 \pm 0.002$ Å^{-1} of the MDC dispersion data at 200 K. Similarly, in (h) the MDC dispersion fit (brown solid line) at 100 K vanishes at $k = 0.398 \pm 0.002$ Å^{-1}, close to the measured $k = 0.4 \pm 0.002$ Å^{-1} of the MDC dispersion data at 100 K. Note that the true Fermi momentum as estimated from the low-T (15-K) data is $k = 0.394 \pm 0.002$ Å^{-1}, so that the deviations are bigger than the momentum resolution $\Delta k \sim 0.004$ Å^{-1}. (i) We plot the temperature dependence of Γ_0 in Fig. 4(a) in Ref. [21]. Here, the temperature dependence data of Γ_0 are fitted with Eq. (6), and η is determined 5.3 ± 2 meV and $\Omega_\Phi = 410 \pm 100$ meV.

VI. CONCLUSION

The main goal of this work is to understand the physical origin of kinks in the dispersion seen in ARPES studies of a wide class of systems. For this purpose we have listed 15 systems of topical interest where ARPES kink data are available. Our focus is on the nodal direction data since the largest volume is available here. We have devised a useful protocol to extract kink parameters from data, where the asymptotic tangents of the kink are used. Using this protocol we have analyzed in detail three families of systems: two synchrotron and one laser ARPES data of cuprate superconductors. The main parameters of the kinks are the energy, momentum, and the dispersion velocities in EDC and MDC scans; these provide a quantitative data set for testing various theoretical proposals for explaining kinks.

We have outlined two competing theories for the origin of kinks, and highlighted their distinctive predictions. One is the electron-boson model, where an Einstein mode of either spin or charge origin couples to the electrons, resulting in a momentum-independent self-energy. This theory gives rise to kinks in the electron dispersion. The other theory is the strong or extreme correlation theory, where the interactions lead to a momentum-dependent self-energy in two dimensions. This theory also gives rise to kinks in the electron dispersion. We expect that other contemporary theories of strong correlations, such as the cellular dynamical mean field theory (CDMFT) [22] method would give comparable results to those of the ECFL theory presented here, which provides the extra convenience of simple analytical expressions.

The predictions of the two theories differ significantly and in experimentally testable ways. Let us summarize the proposed tests.

The boson-mode theory [7] predicts the following:

(1) A kink in the continuous MDC dispersion, located *at* the energy of the localized mode.

(2) A momentum-independent peak at the kink energy, in the spectral function versus energy curve.

(3) A jump discontinuity (rather than a kink) in the EDC dispersion.

(4) The EDC and MDC velocities are identical both *above* and *below* the kink energy.

The (extremely) strongly correlated Fermi liquid theory [7] predicts the following:

(1) A kink in the continuous MDC dispersion, located at a (calculable) *emergent* energy.

(2) No peak in the spectral function at the kink energy.

(3) A kink (rather than a jump discontinuity) in the continuous EDC dispersion.

(4) The EDC and MDC velocities are identical *above* the kink energy.

(5) *Below* the kink energy, the EDC velocity is determined by the two MDC velocities through a simple relation.

It is remarkable that a knowledge of the two MDC dispersions (V_H and V_L) suffices to predict the EDC dispersion below the kink V_H^*, through the relation $V_H^* = \frac{3V_H - V_L}{V_H + V_L} \times V_L$ [see Eq. (10)].

Thus, the parameters obtained from the MDC dispersion enable us to reconstruct the spectral function at low momentum and energy, in both MDC and EDC scans. We have carried out this exercise in three cases above.

It is thus clear that EDC dispersions hold the key to distinguishing between the two competing theories. EDC dispersion data are sparse but exist, the work on OPT Bi2212 from Ref. [4] shown in Fig. 2 presents both EDC and MDC dispersions at 115 K. Its resolution is presumably not optimal since it was an early experiment. Nevertheless, we can use it to make a first pass at comparing the two theories. This data set plotted in Fig. 2 shows that the EDC dispersion is continuous, i.e., has no jump. Further, the EDC higher velocity V_H^* is close to that predicted by the ECFL analysis. The measured spectral function in EDC, overlooking the noise, seems not to have any immovable feature at $E_{\rm kink}$. Thus, all three characteristics noted above appear to be consistent with the ECFL predictions rather than the bosonic mode theory predictions. It is roughly fit by the low-energy parametrized curves as well, where the MDC is seen to be more symmetric than the EDC cuts.

As noted in Table I, the above case OPT Bi2212 is particularly interesting. Low-energy bosonic modes have been observed in neutron scattering [28,29] and in momentum-resolved electron energy loss experiments [27]. In Ref. [27] an MDC dispersion is presented using parameters taken from the bosonic data. This leads to a rather detailed model, and is shown to provide a reasonable fit to the MDC dispersion and the observed kink, but the important EDC dispersion is not displayed.

While we focused attention on dispersion kinks in the nodal direction in this work, the ECFL theory is also valid for other directions; it has a momentum dependence in the self-energy both normal to the Fermi surface and also along the tangent. The ECFL theory applied to the d-wave superconducting state in the t-J model is expected to lead to further interesting results in the future. For now, we note that the observed nodal direction spectra are essentially unchanged at T_c, which makes the nodal direction particularly interesting.

In conclusion, we have presented a current summary of the physics of the kinks in dispersion of cuprate high-T_c superconductors, and given a set of measurements that can distinguish between competing theories. We believe that there is urgent need for further high-resolution EDC data, and also T-dependent scans to explore the rounding of kinks. Using such data one should be able to check the predictions of the theory more thoroughly, and thereby obtain definitive understanding of the origin of low-energy ARPES kinks of strongly correlated matter.

ACKNOWLEDGMENTS

We thank A. Georges and J. Hancock for stimulating discussions. The work at UCSC was supported by the U. S. Department of Energy (DOE), Office of Science, Basic Energy Sciences (BES) under Award No. DE-FG02-06ER46319.

[1] X-J. Zhou, T. Yoshida, A. Lanzara, P. V. Bogdanov, S. A. Kellar, K. M. Shen, W. L. Yang, F. Ronning, T. Sasagawa. T. Kakeshita, T. Noda, H. Eisaki, S. Uchida, C. T. Lin, F. Zhou, J. W. Xiong, W. X. Ti, Z. X. Zhao, A. Fujimori, Z. Hussain, and Z.-X. Shen, Nature (London) **423**, 398 (2003).

[2] P. D. Johnson, T. Valla, A. V. Fedorov, Z. Yusof, B. O. Wells, Q. Li, A. R. Moodenbaugh, G. D. Gu, N. Koshizuka, C. Kendziora, Sha Jian, and D. G. Hinks, Phys. Rev. Lett. **87**, 177007 (2001).

[3] A. Lanzara, P. V. Bogdanov, X. J. Zhou, S. A. Kellar, D. L. Feng, E. D. Lu, T. Yoshida, H. Eisaki, A. Fujimori, K. Kishio, J.-I Shimoyama, T. Noda, S. Uchida, Z. Hussain, and Z.-X. Shen, Nature (London) **412**, 510 (2001).

[4] A. Kaminski, M. Randeria, J. C. Campuzano, M. R. Norman, H. Fretwell, J. Mesot, T. Sato, T. Takahashi, and K. Kadowaki, Phys. Rev. Lett. **86**, 1070 (2001).

[5] T. Sato, H. Matsui, T. Takahashi, H. Ding, H.-B. Yang, S.-C. Wang, T. Fujii, T. Watanabe, A. Matsuda, T. Terashima, and K. Kadowaki, Phys. Rev. Lett. **91**, 157003 (2003).

[6] J. He, W. Zhang, J. M. Bok, D. Mou, L. Zhao, Y. Peng, S. He, G. Liu, X. Dong, J. Zhang, J. S. Wen, Z. J. Xu, G. D. Gu, X. Wang, Q. Peng, Z. Wang, S. Zhang, F. Yang, C. Chen, Z. Xu, H.-Y. Choi, C. M. Varma, and X. J. Zhou, Phys. Rev. Lett. **111**, 107005 (2013).

[7] See Supplemental Material at http://link.aps.org/supplemental/10.1103/PhysRevB.95.165435 for details of the doping dependence of the fit parameters, predictions of the electron-boson coupling model for kinks, predictions of the ECFL theory for kinks.

[8] B. S. Shastry, Phys. Rev. Lett. **107**, 056403 (2011).

[9] B. S. Shastry, Ann. Phys. (NY) **343**, 164 (2014); **373**, 717 (2016).

[10] B. S. Shastry and E. Perepelitsky, Phys. Rev. B **94**, 045138 (2016).

[11] G-H. Gweon, B. S. Shastry, and G. D. Gu, Phys. Rev. Lett. **107**, 056404 (2011).

[12] K. Matsuyama and G-H. Gweon, Phys. Rev. Lett. **111**, 246401 (2013).

[13] D. R. Garcia and A. Lanzara, Advances in Condensed Matter Physics **2010**, 807412 (2010).

[14] T. Yoshida, X. J. Zhou, D. H. Lu, S. Komiya, Y. Ando, H. Eisaki, T. Kakeshita, S. Uchida, Z. Hussain, Z.-X. Shen, and A. Fujimori, J. Phys. Condens. Matter **19**, 125209 (2007).

[15] A. S. Mishchenko, N. Nagaosa, K. M. Shen, Z.-X. Shen, X. J. Zhou, and T. P. Devereaux, Europhys. Lett. **95**, 57007 (2011).

[16] R. J. McQueeney, Y. Petrov. T. Egami, M. Yethiraj, G. Shirane, and Y. Endoh, Phys. Rev. Lett. **82**, 628 (1999).

[17] L. Pintschovius and M. Braden, Phys. Rev. B **60**, R15039(R) (1999).

[18] T. Fukuda, J. Mizuki, K. Ikeuchi, K. Yamada, A. Q. R. Baron, and S. Tsutsui, Phys. Rev. B **71**, 060501(R) (2005).

[19] B. Vignolle, S. M. Hayden, D. F. McMorrow, H. M. Rønnow, B. Lake, C. D. Frost, and T. G. Perring, Nat. Phys. **3**, 163 (2007).

[20] K. Yang, B. P. Xie, D. W. Shen, J. F. Zhao, H. W. Ou, J. Wei, S. Wang, Y. H. Wang, D. H. Lu, R. H. He, M. Arita, S. Qiao, A. Ino, H. Namatame, M. Taniguchi, F. Q. Xu, N. Kaneko, H. Eisaki, and D. L. Feng, Phys. Rev. B **73**, 144507 (2006).

[21] Y. Y. Peng, J.-Q. Meng, L. Zhao, Y. Liu, J.-F. He, G.-D. Liu, X-L. Dong, S.-L. He, J. Zhang, C.-T. Chen, Z.-Y. Xu, and X. J. Zhou, Chin. Phys. Lett. **30**, 067402 (2013).

[22] M. H. Hettler, A. N. Tahvildar-Zadeh, M. Jarrell, T. Pruschke, and H. R. Krishnamurthy, Phys. Rev. B **58**, R7475 (1998); G. Kotliar, S. Y. Savrasov, G. Palsson, and G. Biroli, Phys. Rev. Lett. **87**, 186401 (2001)

[23] W. Meevasana, X. J. Zhou, S. Sahrakorpi, W. S. Lee, W. L. Yang, K. Tanaka, N. Mannella, T. Yoshida, D. H. Lu, Y. L. Chen, R. H. He, Hsin Lin, S. Komiya, Y. Ando, F. Zhou, W. X. Ti, J. W. Xiong, Z. X. Zhao, T. Sasagawa, T. Kakeshita, K. Fujita, S. Uchida, H. Eisaki, A. Fujimori, Z. Hussain, R. S. Markiewicz, A. Bansil, N. Nagaosa, J. Zaanen, T. P. Devereaux, and Z.-X. Shen, Phys. Rev. B **75**, 174506 (2007).

[24] J. Graf, M. d'Astuto, C. Jozwiak, D. R. Garcia, N. L. Saini, M. Krisch, K. Ikeuchi, A. Q. R. Baron, H. Eisaki, and A. Lanzara, Phys. Rev. Lett. **100**, 227002 (2008).

[25] P. V. Bogdanov, A. Lanzara, S. A. Kellar, X. J. Zhou, E. D. Lu, W. J. Zheng, G. Gu, J.-I. Shimoyama, K. Kishio, H. Ikeda, R. Yoshizaki, Z. Hussain, and Z.-X. Shen, Phys. Rev. Lett. **85**, 2581 (2000).

[26] W. Zhang, G. Liu, L. Zhao, H. Liu, J. Meng, X. Dong, W. Lu, J. S. Wen, Z. J. Xu, G. D. Gu, T. Sasagawa, G. Wang, Y. Zhu, H. Zhang, Y. Zhou, X. Wang, Z. Zhao, C. Chen, Z. Xu, and X. J. Zhou, Phys. Rev. Lett. **100**, 107002 (2008).

[27] S. Vig, A. Kogar, V. Mishra, L. Venema, M. S. Rak, A. A. Husain, P. D. Johnson, G. D. Gu, E. Fradkin, M. R. Norman, and P. Abbamonte, arXiv:1509.04230.

[28] H. F. Fong, P. Bourges, Y. Sidis, L. P. Regnault, A. Ivanov, G. D. Gu, N. Koshizuka, and B. Keimer, Nature (London) **398**, 588 (1999).

[29] H. He, Y. Sidis, P. Bourges, G. D. Gu, A. Ivanov, N. Koshizuka, B. Liang, C. T. Lin, L. P. Regnault, E. Schoenherr, and B. Keimer, Phys. Rev. Lett. **86**, 1610 (2001).

[30] S. Ideta, K. Takashima, M. Hashimoto, T. Yoshida, A. Fujimori, M. Kubota, K. Ono, K. Kojima, and S. Uchida, J. Phys.: Conf. Ser. **108**, 1 (2008).

[31] S. Ideta, T. Yoshida, M. Hashimoto, A. Fujimori, H. Anzai, A. Ino, M. Arita, H. Namatame, M. Taniguchi, K. Takashima, K. M. Kojima, and S. Uchida, J. Phys. Conf. Ser. **428**, 012039 (2013).

[32] S. V. Borisenko, A. A. Kordyuk, V. Zabolotnyy, J. Geck, D. Inosov, A. Koitzsch, J. Fink, M. Knupfer, B. Büchner, V. Hinkov, C. T. Lin, B. Keimer, T. Wolf, S. G. Chiuzbăian, L. Patthey, and R. Follath, Phys. Rev. Lett. **96**, 117004 (2006).

[33] W. Reichardt, N. Pyka, L. Pintschovius, B. Hennion, and G. Collin, Phys. C (Amsterdam) **162**, 464 (1989).

[34] L. Pintschovius, D. Reznik, and W. Reichardt, Phys. Rev. B **69**, 214506 (2004).

[35] J. Rossat-Mignod, L. P. Regnault. C. Vettier, P. Bourges, P. Burlet, J. Bossy, J. Y. Henry, and G. Lapertot, Phys. C (Amsterdam) **185**, 86 (1991).

[36] H. A. Mook, M. Yethiraj, G. Aeppli, T. E. Mason, and T. Armstrong, Phys. Rev. Lett. **70**, 3490 (1993).

[37] P. Dai, M. Yethiraj, H. A. Mook, T. B. Lindemer, and F. Doğan, Phys. Rev. Lett. **77**, 5425 (1996).

[38] P. Dai, H. A. Mook, R. D. Hunt, F. Doğan, Phys. Rev. B **63**, 054525 (2001).

[39] I. M. Vishik, N. Barišić, M. K. Chan, Y. Li, D. D. Xia, G. Yu, X. Zhao, W. S. Lee, W. Meevasana, T. P. Devereaux, M. Greven, and Z.-X. Shen, Phys. Rev. B **89**, 195141 (2014).

[40] M. d'Astuto, A. Mirone, P. Giura, D. Colson, A. Forget, and M. Krisch, J. Phys. Condens. Matter **15**, 8827 (2003).

[41] Y. Li, V. Balédent, G. Yu, N. Barišić, K. Hradil, R. A. Mole, Y. Sidis, P. Steffens, X. Zhao, P. Bourges, and M. Greven, Nature **468**, 283 (2010).

[42] Y. Li, G. Yu, M. K. Chan, V. Balédent, Y. Li, N. Barišić, X. Zhao, K. Hradil, R. A. Mole, Y. Sidis, P. Steffens, P. Bourges, and M. Greven, Nat. Phys. **8**, 404 (2012).

[43] M. K. Chan, C. J. Dorow, L. Mangin-Thro, Y. Tang, Y. Ge, M. J. Veit, G. Yu, X. Zhao, A. D. Christianson, J. T. Park, Y. Sidis, P. Steffens, D. L. Abernathy, P. Bourges, and M. Greven, Nat. Commun. **7**, 10819 (2016).

[44] Y. Chen, A. Iyo, W. Yang, A. Ino, M. Arita, S. Johnston, H. Eisaki, H. Namatame, M. Taniguchi, T. P. Devereaux, Z. Hussain, and Z.-X. Shen, Phys. Rev. Lett. **103**, 036403 (2009).

[45] F. Ronning, T. Sasagawa, Y. Kohsaka, K. M. Shen, A. Damascelli, C. Kim, T. Yoshida, N. P. Armitage, D. H. Lu, D. L. Feng, L. L. Miller, H. Takagi, and Z.-X. Shen, Phys. Rev. B **67**, 165101 (2003).

[46] N. Mannella, W. L. Yang, X. J. Zhou, H. Zheng, J. F. Mitchell, J. Zaanen, T. P. Devereaux, N. Nagaosa, Z. Hussain, and Z.-X. Shen, Nature **438**, 474 (2005).

[47] T. Valla, A. V. Fedorov, P. D. Johnson, J. Xue, K. E. Smith, and F. J. DiSalvo, Phys. Rev. Lett. **85**, 4759 (2000).

[48] G. Brusdeylins, C. Heimlich, J. G. Skofronick, J. P. Toennis, R. Vollmer, G. Benedek, and L. Miglio, Phys. Rev. B **41**, 5707 (1990).

[49] J. Schäfer, D. Schrupp, E. Rotenberg, K. Rossnagel, H. Koh, P. Blaha, and R. Claessen, Phys. Rev. Lett. **92**, 097205 (2004).

[50] V. Brouet, A. Nicolaou, M. Zacchigna, A. Taleb-Ibrahimi, P. Le Févre, and F. Bertran, J. Electron Spectrosc. Relat. Phenom. **185**, 146 (2012).